Direct Dynamics Study on Hydrogen Abstraction Reaction of $CF_3CF_2CH_2OH$ with OH Radical

Ying Wang, Jing-yao Liu, Ze-sheng Li,* Li Wang, Jia-yan Wu, and Chia-chung Sun

Institute of Theoretical Chemistry, State Key Laboratory of Theoretical and Computational Chemistry, Jilin University, Changchun 130023, People's Republic of China

Received: November 18, 2005; In Final Form: March 10, 2006

The dual-level direct dynamics method has been employed to investigate the H-abstraction reaction of $CF_3CF_2CH_2OH$ with OH radical, which is predicted to have two classes of possible reaction channels caused by different positions of hydrogen atom attack. The minimum-energy path is calculated at the B3LYP/6-311G(d,p) level, and the energetic information is further refined by the MC-QCISD method. To compare the structures, the other method MPW1K/6-311G(d,p) is also applied to this system. Hydrogen-bonded complexes are presented in the reactant and product sides of the three channels, indicating that each reaction may proceed via an indirect mechanism. The rate constants for each reaction channel are evaluated by canonical variational transition-state theory (CVT) with the small-curvature tunneling correction (SCT) over a wide range of temperatures from 200 to 2000 K. The calculated CVT/SCT rate constants are found to be in good agreement with the available experimental values. The result shows that the variational effect is small, and in the lower-temperature range, the SCT effect is important for each reaction. It is shown that hydrogen abstracted from the $-CH_2-$ position is the major channel, while H-abstraction from the $-OH$ position may be neglected with the temperature increasing.

Introduction

Because of the adverse effects of chlorofluorocarbons (CFCs) and hydrochlorofluorocarbons (HCFCs) on stratospheric ozone depletion[1−3] and global warming,[4−8] an international effort has been made to replace them with environmentally acceptable alternatives. 2,2,3,3,3-Pentafluoropropyl alcohol ($CF_3CF_2CH_2OH$) has been proposed as a cleaning agent to replace the CFCs and HCFCs.[9] Since $CF_3CF_2CH_2OH$ contains no chlorine, it does not destroy the ozone layer, while it will have a contribution to the global warming. Thus, prior to a variety of industrial uses,[10] it is very necessary to evaluate the atmospheric lifetime and the environmental impact of $CF_3CF_2CH_2OH$. The main fate of the $CF_3CF_2CH_2OH$ molecule is expected to be degradation by the reaction with OH radicals.[11] Two experimental studies have been performed to determine the rate constants for the reaction $CF_3CF_2CH_2OH + OH \rightarrow$ products: One is studied using the relative rate method (the temperature range is 298−356 K),[12] and the other is measured by the absolute technique (the temperature range is 250−430 K).[13] The reported results are consistent each other. In ref 12, the authors predicted that the reaction proceeded mainly through H-abstraction from the $-OH$ group, based on the SAR model of Atkinson.[14,15] However, no other theoretical work has addressed the above reaction for the reaction mechanism as well as the branching ratio.

In this study, we employ a dual-level (X//Y) direct dynamics method[16−18] to study the kinetic nature of the title reaction. There are two classes of reaction channels for this reaction: One is hydrogen abstraction from the methylene ($-CH_2-$) position, denoted R1, and the other is hydrogen abstraction from the hydroxyl ($-OH$) position, denoted R2, as follows:

$$CF_3CF_2CH_2OH + OH \rightarrow CF_3CF_2CHOH + H_2O \quad (R1)$$

$$CF_3CF_2CH_2OH + OH \rightarrow CF_3CF_2CH_2O + H_2O \quad (R2)$$

Since the reactant $CF_3CF_2CH_2OH$ has no symmetry, the two hydrogen atoms are not equivalent: One is located between F9 and F10, and the other is behind these two F atoms. As a result, two distinct channels are found and denoted R1a and R1b, respectively. The potential energy surface (PES) information required for the rate constant calculation is obtained directly from density function theory (DFT) calculation, and the high-level single-point energies are calculated by the MC-QCISD[19] method based on low-level B3LYP geometries. Then, the electronic structure information for the stationary points and a series of extra points along the minimum-energy path (MEP) is input into Polyrate 8.4.1[20] to perform the variational transition-state theory (VTST)[21−23] calculations. The comparison between theoretical and experimental rate constants is discussed.

Methods and Calculation Details

All of the electronic structure calculations are carried out by the *Gaussian 03* program.[24] As a reasonable compromise between expense and accuracy, the geometries and frequencies of all the stationary points including reactants, transition states (TSs), products, and complexes are optimized by Becke's three-parameter nonlocal exchange functional[25] with the gradient correction of the Lee, Yang, and Parr[26] method with the 6-311G(d,p) basis set (B3LYP/6-311G(d,p)). The minimum-energy path (MEP) is calculated in mass-weighed Cartesian coordinates using the same electronic structure theory. The single-point energy calculations for the stationary points and a few extra points along the MEP are carried out to establish the electronic potential curve at the multicoefficient correlation method based on quadratic configuration interaction with single and double excitation (MC-QCISD) level.[19] To validate the accuracy of the structure and energies of the stationary points, the geometry optimization calculations are also done using the modified Perdew−Wang one-parameter method for kinetics with the 6-311G(d,p) basis set (MPW1K/6-311G(d,p)),[27] and then, the energies are refined by the MC-QCISD method.[19] For comparison, the bond dissociation energies are also improved by the G3(MP2)[28] method using the B3LYP and MPW1K geom-

* Corresponding author. Fax: +86-431-8498026. E-mail addresses: ljy121@mail.jlu.edu.cn, liujy121@163.com.

10.1021/jp0566818 CCC: $33.50
Published on Web 04/04/2006

etries, respectively. The energy profiles are corrected with interpolated single-point energies (ISPE) method.[29]

On the basis of this initial information (optimized geometries, energies, gradients, and frequencies along the MEP), rate constants are calculated by VTST with the tunneling corrections. The specific form of VTST that we used is canonical variational transition state theory (CVT),[30−32] and the tunneling correction has been considered by the centrifugal-dominant small-curvature semiclassical adiabatic ground-state (CD-SCSAG)[33] method, which is computed with one equal segment in the Boltzmann and θ integrals, and the number of Gauss−Legendre quadrature points is chosen at 40 for computing the Boltzmann average. Also, the sixth-order Lagrangian interpolation is used to obtain the values of the effective mass for the CD-SCSAG tunneling calculation. All the vibrational modes are treated as quantum-mechanical separable harmonic oscillator approximation except for two of them. These two lowest vibrational modes are considered the hindered rotor, and their partition functions are obtained by the hindered rotor approximation of Truhlar and Chuang.[34,35] Here, the model used for the hindered rotor approximation is the torsional mode. The vibrations are treated by rectilinear coordinates at the nonstationary points. During the kinetic calculations, the Euler single-step integrator with a step size of 0.001 $(amu)^{1/2}$ is used to follow the MEP, and the generalized normal-mode analysis is performed every 0.01 $(amu)^{1/2}$ bohr. In the calculation of the electronic partition functions, the two electronic states for OH radicals, with a 140 cm^{-1} splitting in the $^2\Pi$ ground state, are included. All the dynamic calculations are performed by means of the *POLYRATE* program.

Results and Discussion

Stationary Points. The optimized geometric parameters of the reactants, products, transition states, and hydrogen-bonded complexes (HBCs) at the B3LYP/6-311G(d,p) level are shown in Figure 1, along with the available experimental values.[36] It is seen that the theoretical values are in reasonable accord with the experimental geometries of OH and H_2O (given in the parentheses). Because there is no experimental value available for other stationary points, the structures of all stationary points are also calculated at the MPW1K/6-311G(d,p) level, and the corresponding results are shown in the same figure for comparison. It can be seen that the geometries between the two levels are in good mutual agreement. With respect to the transition states, since the transition states TS_{1a} and TS_{1b} are both corresponding to the H-abstraction from methylene ($-CH_2-$) positions, they have similar structures except for the position of the abstracted hydrogen. Now, with TS_{1a} as an example, at the B3LYP/6-311G(d,p) level, the length of the C−H bond which is broken is elongated by about 4.5% in comparison to the C−H equilibrium bond length of $CF_3CF_2CH_2OH$, and the forming bond H−O is longer than the H−O equilibrium bond length in isolated H_2O by 56.1%. In the case of TS_2, the breaking O−H bond is increased by 12.5%, and the forming H−O bond is stretched by 29.6% in comparison to the regular bond length at the B3LYP/6-311G(d,p) level. Whether in TS_{1a}, TS_{1b}, or TS_2, the elongation of the breaking bond (C−H or O−H) is less than that of the forming bond (H−O), indicating that the three transition states are all reactant-like, i.e., the reaction may proceed via an "early" transition state as expected for the exothermic reaction. This early character in the TSs is in keeping with Hammond's postulate. Also, at the MPW1K/6-311G(d,p) level, similar results can be obtained for the three TSs. In addition, because of the high electronegativity of the fluorine atom and the oxygen atom, hydrogen bonds are formed between F and H atoms as well as between H and O atoms. So, the hydrogen-bonded complexes with energies less than the reactants or products are located at the entrance and exit channels of reactions R1 and R2, respectively, which mean that the reactions may proceed via an indirect mechanism. In the complexes, the hydrogen-bond lengths of O···H and H···F are all less than the sum of their van der Waals radii (2.72 and 2.67 Å), and the other bond lengths are very close to those of the reactants and products. For example, in complex CR_{1a}, the bond distances of O13···H4 and H14···F9 are 2.03 and 2.28 Å, respectively, less than the sum of their van der Waals radii.

The harmonic vibrational frequencies are calculated to confirm the stationary nature and to make zero-point energy (ZPE) corrections. All of the minima including reactants, products, and complexes possess only real frequencies, while the transition states are confirmed by normal-mode analysis to have one and only one imaginary frequency corresponding to the stretching modes of the coupling between breaking and forming bonds. The calculated frequencies at the B3LYP level are displayed in Table 1, along with the experimental data of OH[37] and H_2O.[37]

The calculated reaction enthalpies (ΔH°_{298}) of the three reaction channels at several levels are listed in Table 2. It is found that the reactions are all exothermic, with reaction enthalpies of −25.35 and −12.77 kcal/mol for R1 and R2, respectively, at the MC-QCISD//B3LYP level, which agree with the results obtained at the MC-QCISD level based on MPW1K geometries (−24.72 kcal/mol for R1 and −12.38 kcal/mol for R2). The largest deviation between the two methods is only 0.7 kcal/mol.

A schematic potential energy surface of the title reaction obtained at the MC-QCISD//B3LYP/6-311G(d,p) level with zero-point energy (ZPE) corrections is plotted in Figure 2. The energy of the reactant is set to zero for reference. For reaction channels R1 and R2, the hydrogen-bonded complexes are located at the reactant entrance. The energies of CR_{1a}, CR_{1b}, and CR_2 are lower than those of the reactants by 3.10, 4.62, and 6.61 and 0.90, 1.21, and 1.40 kcal/mol at the B3LYP and MC-QCISD//B3LYP levels, respectively. Then, starting from the complex, each reaction passes through a reactant-like transition state to form another complex with relative energies of 0.44, 6.69, and 0.81 kcal/mol below the products of CF_3CF_2CHOH (-1a and -1b) + H_2O and $CF_3CF_2CH_2O$ + H_2O at the MC-QCISD//B3LYP level. The potential barriers with ZPE corrections are −3.52 and −3.61 kcal/mol for H-abstraction from the $-CH_2-$ position at the B3LYP/6-311G(d,p) level, while at the MC-QCISD//B3LYP level, they increase by about 6.0 kcal/mol. In the case of R2, the hydrogen abstraction from the −OH position involves a barrier of 3.82 kcal/mol with respect to the reactants at the MC-QCISD//B3LYP level, which is higher than the ones of R1a and R1b by 1.34 and 1.74 kcal/mol, respectively. Meantime, R2 is less exothermic than R1 by about 12 kcal/mol. So, reaction R2 may be thermodynamically less favorable than R1a and R1b, i.e., the title reaction will proceed mainly through the channel of H-abstraction from the $-CH_2-$ group, while the hydrogen abstraction from hydroxyl is a minor channel. It should be noted that we have also performed the barrier height calculations at the MC-QCISD//MPW1K level. The corresponding results are shown in Table 2. Seen from Table 2, we can find that the energy barriers for the three channels obtained at the MPW1K level are quite different from those at the B3LYP level, but they show good agreement with each other when the highly correlated and more accurate method MC-QCISD is used with the maximum deviation within 0.8 kcal/mol. The ΔE(0 K) calculated at the

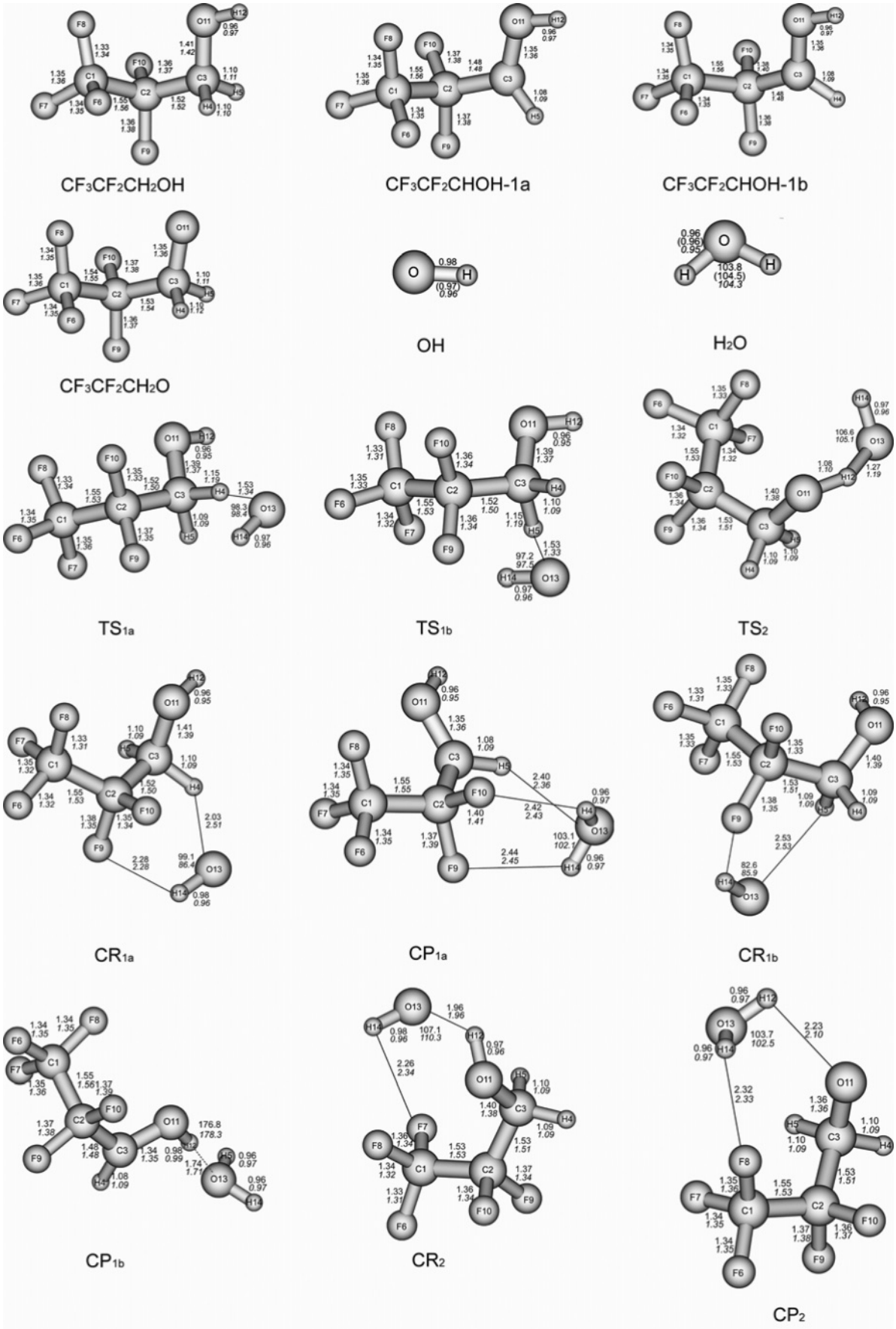

Figure 1. Optimized geometries parameters (in Å and deg) of the reactants, products, transition states (TSs), and hydrogen-bond complexes at the B3LYP/6-311G(d,p) and MPW1K/6-311G(d,p) levels, as well as available experimental ones. The values in italic and in the parentheses are obtained at the MPW1K/6-311G(d,p) level and the experimental ones.[36]

TABLE 1: Calculated Frequencies (cm^{-1}) of the Stationary Points at the B3LYP/6-311G (d, p) Level, along with the Experimental Values

species	frequencies
$CF_3CF_2CH_2OH$	48, 111, 148, 190, 224, 262, 333, 352, 385, 463, 518, 583, 619, 635, 766, 941, 1097, 1105, 1141, 1184, 4211, 1228, 1244, 1280, 1379, 1477, 1507, 3007, 3055, 3856
CF_3CF_2CHOH-1a	49, 85, 174, 214, 250, 297, 343, 367, 385, 434, 467, 532, 582, 630, 680, 774, 1027, 1106, 1178, 1197, 1207, 1244, 1275, 1308, 1491, 3202, 3844
CF_3CF_2CHOH-1b	34, 86, 182, 213, 225, 285, 341, 370, 383, 435, 472, 525, 583, 644, 650, 769, 1028, 1085, 1177, 1198, 1208, 1219, 1279, 1352, 1490, 3198, 3844
$CF_3CF_2CH_2O$	40, 105, 178, 215, 245, 314, 353, 383, 455, 511, 544, 582, 642, 665, 769, 989, 1092, 1134, 1169, 1192, 1212, 1244, 4338, 1357, 1398, 2928, 2968
OH	3705 (3735)[a]
H_2O	1638, 3810, 3907 (1595, 3657, 3756)[a]
TS_{1a}	131i, 40, 62, 90, 144, 198, 216, 225, 261, 268, 343, 360, 384, 462, 523, 582, 616, 631, 677, 711, 933, 1094, 1121, 1140, 1186, 1206, 1231, 1259, 1280, 1344, 1397,1469, 2100, 3058, 3726, 3844
TS_{1b}	140i, 33, 50, 93, 132, 191, 197, 225, 263, 284, 332, 352, 387, 465, 517, 580, 616, 627, 672, 765, 957, 1088, 1111, 1141, 1172, 1205, 1221, 1237, 1243, 1372, 1455, 1460, 2077, 3022, 3732, 3839
TS_2	1032i, 57, 74, 99, 148, 203, 218, 256, 257, 331, 351, 383, 451, 465, 524, 582, 610, 648, 766, 773, 920, 1078, 1109, 1138, 1190, 1201, 1217, 1263, 1311, 1378, 1413, 1447, 1622, 3016, 3090, 3772
CR_{1a}	27, 33, 53, 109, 125, 178, 193, 221, 230, 366, 336, 340, 357, 386, 463, 520, 583, 620, 633, 766, 944, 1086, 1110, 1135, 1185, 1211, 1228, 1255, 1282, 1377, 1469, 1487, 2912, 3048, 3711, 3853
CP_{1a}	46, 59, 75, 83, 131, 178, 198, 220, 265, 282, 323, 346, 370, 394, 410, 467, 514, 570, 594, 621, 665, 768, 987, 1074, 1154, 1201, 1211, 1222, 1277, 1380, 1501, 1658, 3193, 3805, 3843, 3889
CR_{1b}	42, 53, 81, 108, 125, 164, 194, 225, 246, 311, 345, 357, 361, 385, 457, 526, 579, 611, 347, 764, 929, 1072, 1100, 1114, 1181, 1196, 1215, 1265, 1368, 1407, 1435, 1497, 3045, 3108, 3703, 3838
CP_{1b}	32, 44, 65, 83, 116, 159, 212, 224, 266, 280, 305, 336, 357, 392, 432, 469, 534, 582, 631, 686, 776, 867, 1025, 1112, 1184, 1197, 1203, 1258, 1301, 1369, 1520, 1631, 3195, 3507
CR_2	51, 55, 73, 99, 165, 196, 218, 219, 252, 310, 328, 352, 385, 458, 485, 527, 582, 614, 644, 766, 916, 1087, 1111, 1127, 2291, 1198, 1214, 1267, 1312, 1387, 1444, 1482, 3028, 3103, 3603, 3737
CP_2	49, 62, 94, 120, 148, 189, 196, 216, 249, 277, 318, 353, 383, 410, 460, 524, 580, 592, 655, 754, 784, 1017, 1087, 1135, 1179, 1187, 1206, 1244, 1343, 1360, 1410, 1642, 2949, 3012, 3805, 3894

[a] From ref 37.

TABLE 2: Enthalpies and Relative Energies (in kcal/mol) Calculated at Various Levels

	ΔH°_{298}			ΔE		
method	R1a	R1b	R2	R1a	R1b	R2
B3LYP/6-311G(d,p)	−21.46	−21.32	−13.69	−3.52	−3.61	−6.61
MPW1K/6-311G(d,p)	−21.77	−21.66	−12.60	0.59	0.59	0.60
MC-QCISD//B3LYP	−25.35	−25.03	−12.77	2.48	2.08	3.82
MC-QCISD//MPW1K	−24.72	−24.32	−12.38	1.66	1.61	4.24

MC-QCISD/MPW1K level also indicates that the major channel is H-abstraction from the $-CH_2-$ position. Unfortunately, our result is quite different from the estimation of SAR (structure−activity relationships) by Chen and Fukuda et al.[12] In that paper, they think the H-atom abstraction from the O−H bond of $CF_3CF_2CH_2OH$ producing the $CF_3CF_2CH_2O$ radical, i.e., channel R2, is the main degraded channel. To further prove which is more reasonable, we use another method to estimate the results, i.e., by calculating the bond dissociation energies (BDEs) of the breaking C−H bond and the O−H bond at the MC-QCISD//B3LYP level. To avoid the error caused by method, MC-QCISD//MPW1K, G3(MP2)//B3LYP, and G3(MP2)//MPW1K are also applied to calculated the bond dissociation energies. The results are all listed in Table 3. It is clearly seen that the results obtained at four higher levels are mutually consistent, and the dissociation energy of the bond O−H is higher than that of the bond C−H by about 10 kcal/mol, which suggests that H-abstraction from the $-CH_2-$ position should predominate the reaction. This conclusion can be supported by the rate constant calculation in the following section.

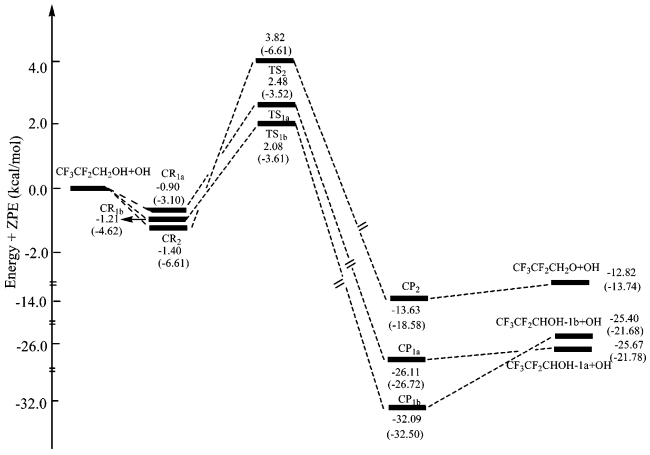

Figure 2. Schematic potential energy surface for the reaction $CF_3CF_2CH_2OH + OH$. Relative energies with ZPE at the MC-QCISD//B3LYP/6-311G(d,p) level are in kcal/mol.

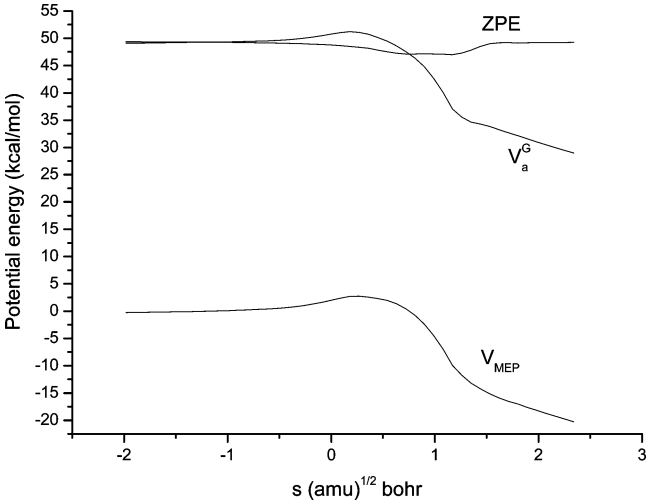

Figure 3. Classical potential energy curve (V_{MEP}), ground-state vibrationally adiabatic energy curve (V_a^G), and zero-point energy curve (ZPE) as functions of s $(amu)^{1/2}$ bohr at the MC-QCISD//B3LYP/6-311G(d,p) level for reaction $CF_3CF_2CH_2OH + OH \rightarrow CF_3CF_2CHOH$-1b + H_2O.

TABLE 3: Bond Dissociation Energies (in kcal/mol) at the MC-QCISD//B3LYP, G3(MP2)//B3LYP, MC-QCISD//MPW1K, and G3(MP2)//MPW1K Levels

	C−H4	C−H5	O−H
MC-QCISD//B3LYP	97.33	97.66	109.92
G3(MP2)//B3LYP	96.57	96.87	106.51
MC-QCISD//MPW1K	96.32	96.72	108.66
G3(MP2)//MPW1K	95.59	95.94	105.31

Reaction Path Properties. The minimum-energy path (MEP) is calculated by the intrinsic reaction coordinate (IRC) theory at the B3LYP/6-311G(d,p) level from the transition state to the reactant and product, respectively. The potential profiles are further refined at the MC-QCISD level. Figure 3 shows the plots of the classical potential energy, V_{MEP}, the ground-state vibrational adiabatic potential energy, V_a^G, and the zero-point energy

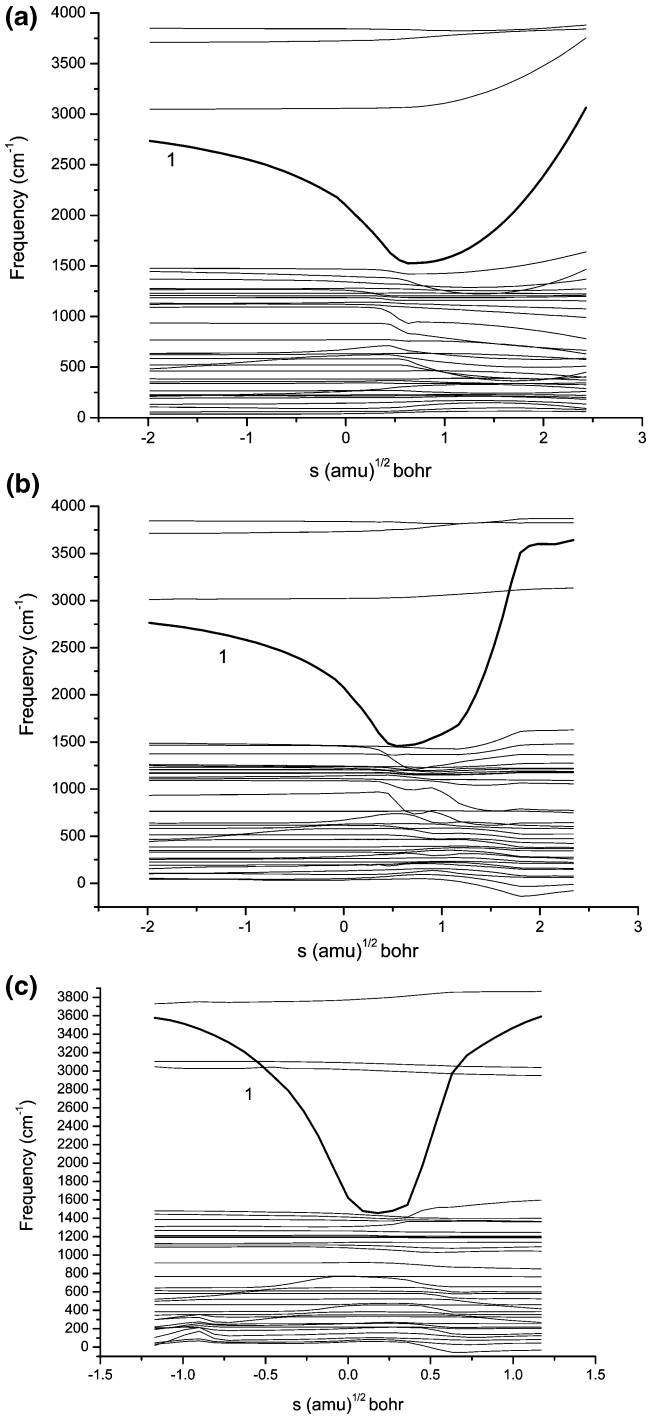

Figure 4. Changes of the generalized normal-mode vibrational frequencies as functions of s (amu)$^{1/2}$ bohr at the MC-QCISD//B3LYP/6-311G(d,p) level for reactions: (a) $CF_3CF_2CH_2OH + OH \rightarrow CF_3CF_2CHOH$-1a + H_2O; (b) $CF_3CF_2CH_2OH + OH \rightarrow CF_3CF_2CHOH$-1b + H_2O; (c) $CF_3CF_2CH_2OH + OH \rightarrow CF_3CF_2CH_2O + H_2O$.

curves (ZPE(s)) for R1b as functions of the intrinsic reaction coordinate (s) at the MC-QCISD//B3LYP level, where $V_a^G = V_{MEP} + ZPE$. Because of the similarity, the corresponding plots for R1a and R2 are depicted in Figure S1 (Supporting Information). As can be seen from Figure 3, the ZPE curve shows very little change with *s*, and the V_{MEP} and V_a^G curves are similar in shape. This analysis indicates that, for the three reactions, the variational effect will be small or almost negligible.

Figure 4 shows the variation of the generalized normal-mode vibrational frequencies along the MEP for reactions R1a, R1b, and R2. In Figure 4, in the negative limit of *s* ($s = -\infty$), the frequencies are associated with those of the reactant complex,

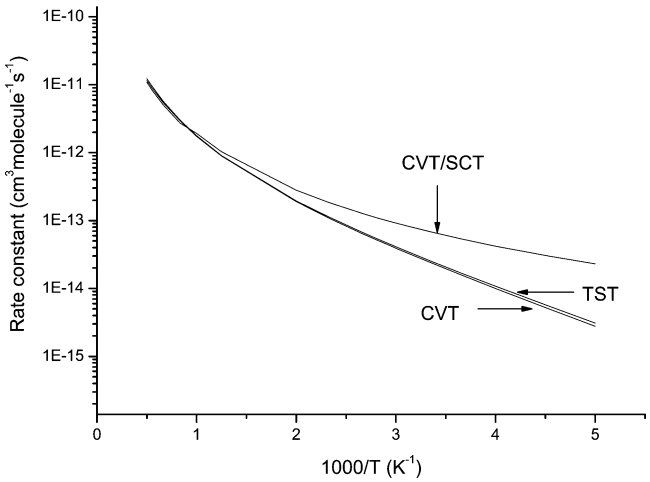

Figure 5. Plots of the TST, CVT, and CVT/SCT rate constants calculated at the MC-QCISD//B3LYP/6-311G(d,p) level vs 1000/*T* between 200 and 2000 K for reaction $CF_3CF_2CH_2OH + OH \rightarrow CF_3CF_2CHOH$-1b + H_2O.

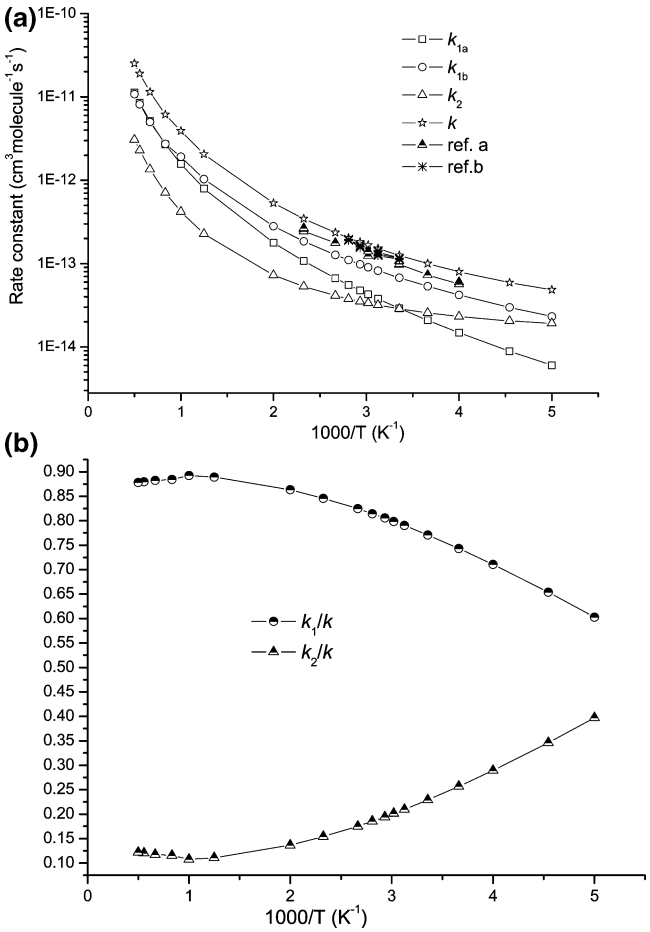

Figure 6. (a) The total rate constants *k* and each channel rate constant k_{1a}, k_{1b}, or k_2, and available experimental values (in cm^3 molecule^{-1} s^{-1}) as functions of the reciprocal of the temperature (K) over the temperature range 200−2000 K for reaction $CF_3CF_2CH_2OH + OH \rightarrow$ products. (b) Calculated branching ratios vs 1000/*T* between 200 and 2000 K for reaction $CF_3CF_2CH_2OH + OH \rightarrow$ products.

and in the product region at about 2.0 (amu)$^{1/2}$ bohr, the frequencies correspond to those of the product complex. In the process of the reaction, most of those frequencies do not change significantly in going from the reactants to the products, but the frequency of mode 1, shown as the solid line in bold in Figure 4, which connects the stretching vibrational mode of the breaking and forming bonds, has a dramatic drop as the reaction

TABLE 4: Calculated Rate Constants (in cm^3 molecule^{-1} s^{-1}) for the Reaction CF3CF$_2$CH2OH + OH → Products in the Temperature Range 200−2000 K at the MC-QCISD//B3LYP/6-311G(d,p) Level of Theory.

T (K)	R1a CVT/SCT	R1b CVT/SCT	R2 CVT/SCT	total CVT	total CVT/SCT	total CVT/ZCT	exptl.
200	6.03×10^{-15}	2.31×10^{-14}	1.92×10^{-14}	3.91×10^{-15}	4.83×10^{-14}	2.24×10^{-14}	
220	8.9×10^{-15}	2.98×10^{-14}	2.05×10^{-14}	7.14×10^{-15}	5.92×10^{-14}	3.06×10^{-14}	
250	1.48×10^{-14}	4.2×10^{-14}	2.31×10^{-14}	1.50×10^{-14}	7.99×10^{-14}	4.69×10^{-14}	$(6.42 \pm 0.27) \times 10^{-14}$ [b] $(6.31 \pm 0.21) \times 10^{-14}$ [b]
273	2.08×10^{-14}	5.33×10^{-14}	2.56×10^{-14}	2.40×10^{-14}	9.97×10^{-14}	6.30×10^{-14}	$(8.01 \pm 0.27) \times 10^{-14}$ [b]
298	2.9×10^{-14}	6.76×10^{-14}	2.87×10^{-14}	3.72×10^{-14}	1.25×10^{-13}	8.44×10^{-14}	$(1.05 \pm 0.05) \times 10^{-13}$ [b] $(0.978 \pm 0.04 \times 10^{-13}$ [b] $(0.974 \pm 0.04 \times 10^{-13}$ [b] $(1.16 \pm 0.08) \times 10^{-13}$ [a] $(1.15 \pm 0.08) \times 10^{-13}$ [a] $(1.12 \pm 0.08) \times 10^{-13}$ [a]
320	3.78×10^{-14}	8.21×10^{-14}	3.18×10^{-14}	5.23×10^{-14}	1.52×10^{-13}	1.07×10^{-13}	$(1.38 \pm 0.10) \times 10^{-13}$ [a] $(1.25 \pm 0.09) \times 10^{-13}$ [a] $(1.31 \pm 0.09) \times 10^{-13}$ [a] $(1.43 \pm 0.10) \times 10^{-13}$ [a] $(1.28 \pm 0.09) \times 10^{-13}$ [a]
331	4.27×10^{-14}	9.01×10^{-14}	3.35×10^{-14}	6.12×10^{-14}	1.66×10^{-13}	1.20×10^{-13}	$(1.21 \pm 0.04) \times 10^{-13}$ [b]
341	4.76×10^{-14}	9.78×10^{-14}	3.51×10^{-14}	7.02×10^{-14}	1.81×10^{-13}	1.32×10^{-13}	$(1.55 \pm 0.11) \times 10^{-13}$ [a] $(1.65 \pm 0.12) \times 10^{-13}$ [a] $(1.60 \pm 0.12) \times 10^{-13}$ [a] $(1.62 \pm 0.11) \times 10^{-13}$ [a]
356	5.55×10^{-14}	1.1×10^{-13}	3.77×10^{-14}	8.50×10^{-14}	2.03×10^{-13}	1.52×10^{-13}	$(1.93 \pm 0.14) \times 10^{-13}$ [a] $(1.96 \pm 0.14) \times 10^{-13}$ [a] $(1.90 \pm 0.14) \times 10^{-13}$ [a] $(1.95 \pm 0.14) \times 10^{-13}$ [a]
375	6.67×10^{-14}	1.27×10^{-13}	4.12×10^{-14}	1.06×10^{-13}	2.35×10^{-13}	1.81×10^{-13}	$(1.76 \pm 0.07) \times 10^{-13}$ [b]
430	1.07×10^{-13}	1.85×10^{-13}	5.32×10^{-14}	1.87×10^{-13}	3.45×10^{-13}	2.81×10^{-13}	$(2.34 \pm 0.09) \times 10^{-13}$ [b] $(2.36 \pm 0.07) \times 10^{-13}$ [b]
500	1.78×10^{-13}	2.81×10^{-13}	7.26×10^{-14}	3.37×10^{-13}	5.32×10^{-13}	4.54×10^{-13}	
800	7.96×10^{-13}	1.03×10^{-12}	2.28×10^{-13}	1.71×10^{-12}	2.05×10^{-12}	1.92×10^{-12}	
1000	1.57×10^{-12}	1.92×10^{-12}	4.20×10^{-13}	3.47×10^{-12}	3.91×10^{-12}	3.73×10^{-12}	
1200	2.7×10^{-12}	2.72×10^{-12}	7.07×10^{-13}	6.01×10^{-12}	6.13×10^{-12}	5.92×10^{-12}	
1500	5.13×10^{-12}	5.01×10^{-12}	1.35×10^{-12}	1.15×10^{-11}	1.15×10^{-11}	1.12×10^{-11}	
1800	8.51×10^{-12}	8.17×10^{-12}	2.28×10^{-12}	1.91×10^{-11}	1.90×10^{-11}	1.87×10^{-11}	
2000	1.13×10^{-11}	1.08×10^{-11}	3.07×10^{-12}	2.54×10^{-11}	2.52×10^{-11}	2.47×10^{-11}	

[a] From ref 12. [b] From ref 13.

proceeds. Therefore, mode 1 is referred to as the "reactive mode". These behaviors are known to be typical of the hydrogen transfer reaction.[38] Also, we can see from Figure 4a−c that the lowest harmonic frequencies for R1a are all real, and the imaginary frequencies for both R1b and R2 are much smaller, with the largest one less than 138i cm^{-1} for R1b and 55i cm^{-1} for R2 at the product sides. Thus, it is reasonable for these reactions to perform generalized normal-mode analysis using rectilinear coordinates in the present study.

Rate Constants Calculation. Dual-level dynamics calculations of the hydrogen abstraction reactions R1a, R1b, and R2 are carried out with VTST-ISPE approach, in which six extra MC-QCISD//B3LYP/6-311G(d,p) energies are used to refine the classical energy profile obtained at the B3LYP level. The rate constants are evaluated by the conventional transition state theory (TST) and canonical variation transition state theory (CVT) over a wide temperature region from 200 to 2000 K. Tunneling is included by means of the small-curvature tunneling (SCT) correction. The plots of TST, CVT, and CVT/SCT rate constants for channel R1b is shown in Figure 5, and the corresponding plots of R1a and R2 are shown in Figure S2 (Supporting Information) as functions of the reciprocal of the temperature. The total rate constants for the reaction are obtained from the sum of the individual rate constants associated with the three channels ($k = k_{1a} + k_{1b} + k_2$). The CVT/SCT rate constants together with the corresponding experimental data are displayed in Table 4 and Figure 6a.

Seen from Figure 5, the TST and CVT rate constants for H-abstraction from the -CH_2− position (R1b) have a little discrepancy, but are still very close in the lower temperature, and with the temperature increasing, they have almost the same values. The same observation can be made for the other two reaction channels. This indicates that, for H-abstraction from either the C−H or the O−H position, the variational effect is negligible. On the other hand, we find that the small-curvature effect plays an important role at low temperature, while it can be negligible with the increase of temperature in the rate constant calculation. For example, the k(CVT/SCT)/k(CVT) ratios are 8.31 and 0.94 at 200 and 2000 K for R1b, respectively. To further estimate the tunneling effect, we also calculated the rate constant with the ZCT (zero-curvature tunneling) method. The corresponding total rate constants are listed in Table 4. It can be seen that the CVT/SCT rate constants are greater than the CVT/ZCT values at lower temperature, which means that the tunneling factor in the SCT method enlarges the rate constants. For example, at 200 K, the CVT/SCT rate constant is 4.83×10^{-14} cm^3 molecule^{-1} s^{-1}, whereas the CVT/ZCT rate constant is 2.24×10^{-14} cm^3 molecule^{-1} s^{-1}. The former is 2.2 times larger than the latter. While with the temperature increasing, the CVT/ZCT rate constants are asymptotic to the CVT/SCT rate constants, for example, at 2000 K the CVT/SCT and CVT/ZCT rate constants are 2.52×10^{-11} and 2.47×10^{-11} cm^3 molecule^{-1} s^{-1}, respectively. By comparing the CVT, CVT/ZCT, and CVT/SCT results presented in Table 4, we found that the CVT/SCT rate constants are in better agreement with the experimental values with factors of 1.2 at 250 K and 1.4 at 430 K. Thus, the SCT correction is considered for the reaction. Furthermore, the calculated CVT/SCT rate constants in the 250−430 K range are fitted to be $k = 2.34 \times 10^{-12} \exp(-862/T)$ cm^3 molecule^{-1} s^{-1}, which is in reasonably good accord with the expression $k = (1.40 \pm 0.27) \times 10^{-12} \exp[(-780 \pm 60)/T]$ cm^3 molecule^{-1} s^{-1} proposed by Tokuhashi et al.[13] In the 298−356 K range, the fitted expression of $k = 2.40 \times 10^{-12} \exp(-882/T)$ cm^3 molecule^{-1} s^{-1} also agrees well with the

expression of $k = (2.27^{+1.15}_{-0.76}) \times 10^{-12} \exp[(-900 \pm 70)/T]$ cm^3 molecule^{-1} s^{-1} proposed by Chen et al.[12]

Figure 6b shows the temperature dependence of the branching ratios. It can be found that at the lower temperatures the contribution of channels R1 and R2 should both be taken into account, with the ratio of $k_1/k_2 = 3{:}2$ at 200 K, but with the temperature increasing, channel R1 plays a more important role in the total reaction, and the contribution of channel R2 could be neglected at higher temperatures. Thus, for the multichannel reaction, the dominant reaction channel is H-abstraction from the methylene position leading to the product CF_3CF_2CHOH.

Since there are few data available at higher temperatures, for offering further information concerning this hydrogen abstraction reaction, the three-parameter fit for the CVT/SCT rate constants within 200−2000 K gives the expression as follows (in cm^3 molecule^{-1} s^{-1}):

$$k = 6.45 \times 10^{-21} T^{2.91} \exp(74.9/T)$$

Conclusions

In this paper, we employed a dual-level dynamics method to study the hydrogen abstraction reaction $CF_3CF_2CH_2OH + OH$. Two classes of H-abstraction reaction channels are identified. The potential energy surface information is obtained at the B3LYP/6-311G(d,p) and MPW1K/6-311G(d,p) levels, and the higher-level energies of the stationary points and a few extra points along the MEP are calculated by MC-QCISD theory. The theoretical rate constants for each reaction channel are calculated by canonical variational transition state theory (CVT) with the small-curvature tunneling correction (SCT) at the MC-QCISD//B3LYP level. The results are consistent with the experimental values in the corresponding measured temperature regions. For R1a, R1b, and R2, the variational effect has little contribution in the whole temperature ranges, while the SCT correction plays an important role in the lower temperature regions. The bond dissociation energies of are calculated by MC-QCISD and G3(MP2) based on B3LYP/6-311G(d,p) and MPW1K/6-311G(d,p) geometries to further confirm that for the title reaction H-abstraction from the methylene position is the major reaction channel, while H-abstraction from the hydroxyl position may play a lesser role with the temperature increasing.

Acknowledgment. The authors would like to thank Professor Donald G. Truhlar for providing the *POLYRATE* 8.4.1 program. This work was supported by the National Natural Science Foundation of China (20303007, 20333050, 20073014), the Doctor Foundation by the Ministry of Education, and the Foundation for University Key Teacher by the Ministry of Education, the Key Subject of Science and Technology by the Ministry of Education of China, and the Innovational Foundation by Jilin University.

Supporting Information Available: Additional graphical data. This material is available free of charge via the Internet at http://pubs.acs.org.

References and Notes

(1) Molina, M. J.; Rowland, F. S. *Nature (London)* **1974**, *249*, 810.

(2) Hammitt, J. K.; Camm, F.; Connell, P. S.; Mooz, W. E.; Wolf, K. A.; Wuebbles, D. J.; Bamezoi, A. *Nature (London)* **1987**, *330*, 711.

(3) Rebbert, R. E.; Ausloos, P. J. *J. Photochem.* **1975**, *4*, 419; **1976/1977**, *6*, 265.

(4) Hanel, R. A. *J. Geophys. Res.* **1972**, *77*, 2629.

(5) Houghton, J. T., Meira Filho, L. G., Callender, B. A., Harris, N., Kattenberg, A., Maskell, K., Eds. *WMO/UNEP, Climate Change 1995, The IPCC Scientific Assessment*; Cambridge University Press: Cambridge, 1996.

(6) Fisher, D. A.; Hales, C. H.; Wang, W. C.; Ko, M. K. W.; Sze, N. D. *Nature (London)* **1990**, *344*, 513.

(7) *WMO/UNEP, Atmospheric Ozone: 1985*; World Meterological Organization Global Ozone Research and Monitoring Project, Report No. 16; World Meteorological Organization: Geneva, Switzerland, 1986.

(8) *Scientific Assessment of Stratospheric Ozone: 1989*; World Meteorological Organization Global Ozone Research and Monitoring Project, Report No. 20; World Meterological Organization: Geneva, Switzerland, 1990; Vol. 2 Appendix AFEAS Report.

(9) Fluorocarbon Manufacturers Association, Eds.; *Tokutei Furon Siyousakugen Manyuaru* (in Japanese); Tokyo, 1990.

(10) Kissa, E., Schick, M. J., Fowkes, F. M., Eds. *Fluorinated Surfactants, Synthesis, Properties, and Applications*; Marcel Dekker: New York, 1994.

(11) *Scientific Assessment of Ozone Depletion: 1994*; UNEP/WMO Global Ozone Research and Monitoring Project, Report No. 37; World Meterological Organization: Geneva, 1995.

(12) Chen, L.; Fukuda, K.; Takenaka, N.; Bandow, H.; Maeda, Y. *Int J. Chem. Kinet.* **2000**, *32*, 73.

(13) Tokuhashi, K.; Nagai, H.; Takahashi, A.; Kaise, M.; Kondo, S.; Sekiya, A.; Takahashi, M.; Gotoh, Y.; Suga, A. *J. Phys. Chem. A* **1999**, *103*, 266.

(14) Kwok, E. S. C.; Atkinson, R. *Atmos. Environ.* **1995**, *29*, 1685.

(15) Atkinson, R. *Chem. Rev.* **1986**, *86*, 69; *Int. J. Chem. Kinet.* **1986**, *18*, 555; *Int. J. Chem. Kinet.* **1987**, *19*, 799.

(16) Truhlar, D. G. *Direct Dynamics Method for the Calculation of Reaction Rates: The Reaction Path, in The Reaction Path in chemistry: current Approaches and Perspectives*; Heidrich, Ed.; Kluwer: Dordrecht, The Netherlands, 1995; p 229.

(17) Truhlar, D. G.; Garrett, B. C.; Klippenstein, S. J. *J. Phys. Chem.* **1996**, *100*, 12771.

(18) Hu, W. P.; Truhlar, D. G. *J. Am. Chem. Soc.* **1996**, *118*, 860.

(19) Patton, L. F.; Truhlar, D. G. *J. Phys. Chem. A* **2000**, *104*, 6111.

(20) Chuang, Y. Y.; Corchado, J. C.; Fast, P. L.; Villa, J.; Hu, W. P.; Liu, Y. P.; Lynch, G. C.; Jackels, C. F.; Nguyen, K. A.; Gu, M. Z.; Rossi, I.; Coitino, E. L.; Clayton, S.; Melissas, V. S.; Lynch, B. J.; Steckler, R.; Garrett, B. C.; Isaacson, A. D.; Truhlar, D. G. *POLYRATE*, v. 8.4.1; University of Minnesota: Minneapolis, 2000.

(21) Truhlar, D. G.; Garrett, B. C. *Acc. Chem. Res.* **1980**, *13*, 440.

(22) Truhlar, D. G.; Isaacson, A. D.; Garrent, B. C. *The Theory of Chemical Reaction Dynamics*; Baer, M., Ed.; CRC Press: Boca Raton, FL, 1985; p 65.

(23) Truhlar, D. G.; Garrett, B. C. *Annu. Rev. Phys. Chem.* **1984**, *35*, 159.

(24) Frisch, M. J.; Truck, G. W.; Schlegel, H. B.; Scuseria, G. E.; Robb, M. A.; Cheeseman, J. R.; Zakrzewski, V. G.; Montgomery, J. A., Jr.; Stratmann, R. E.; Burant, J. C.; Dapprich, S.; Millam, J. M.; Daniels, A. D.; Kudin, K. N.; Strain, M. C.; Farkas, O.; Tomasi, J.; Barone, V.; Cossi, M.; Cammi, R.; Mennucci, B.; Pomelli, C.; Adamo, C.; Clifford, S.; Ochterski, J.; Petersson, G. A.; Ayala, P. Y.; Cui, Q.; Morokuma, K.; Malick, D. K.; Rabuck, A. D.; Raghavachari, K.; Foresman, J. B.; Cioslowski, J.; Ortiz, J. V.; Boboul, A. G.; Stefnov, B. B.; Liu, G.; Liaschenko, A.; Piskorz, P.; Komaromi, L.; Gomperts, R.; Martin, R. L.; Fox, D. J.; Keith, T.; Al-Laham, M. A.; Peng, C. Y.; Nanayakkara, A.; Gonzalez, C.; Challacombe, M.; Gill, P. M. W.; Johnson, B.; Chen, W.; Wong, M. W.; Andres, J. L.; Gonzalez, C.; Head-Gordon, M.; Replogle E. S.; Pople, J. A. *Gaussian 03*, revision A.1; Guassian, Inc.: Pittsburgh, PA, 2003.

(25) Becker, A. D. *J. Chem. Phys.* **1993**, *98*, 1372.

(26) Lee, C.; Yang, W.; Parr, R. G. *Phys. Rev. B* **1988**, *37*, 785.

(27) Lynch, B. J.; Fast, P. L.; Harris, M.; Truhlar, D. G. *J. Phys. Chem. A* **2000**, *104*, 21.

(28) Curtiss, L. A.; Redfern, P. R. *J. Chem. Phys.* **1999**, *110*, 4703.

(29) Chuang, Y. Y.; Corchado, J. C.; Truhlar, D. G. *J. Phys. Chem.* **1999**, *103*, 1140.

(30) Garrett, B. C.; Truhlar, D. G. *J. Chem. Phys.* **1979**, *70*, 1593.

(31) Garrett, B. C.; Truhlar, D. G. *J. Am. Chem. Soc.* **1979**, *101*, 4534.

(32) Garrett, B. C.; Truhlar, D. G.; Grev, R. S.; Magnuson, A. W. *J. Phys. Chem.* **1980**, *84*, 1730; **1983**, *87*, 4534 (erratum).

(33) Liu, Y. P.; Lynch, G. C.; Truong, T. N.; Lu, D. H.; Truhlar, D. G.; Garrett, B. C. *J. Am. Chem. Soc.* **1993**, *115*, 2408.

(34) Truhlar, D. G. *J. Comput. Chem.* **1991**, *12*, 266.

(35) Chuang, Y. Y.; Truhlar, D. G. *J. Chem. Phys.* **2000**, *112*, 1221.

(36) Lide, D. R. *CRC Handbook of Chemistry and Physics*, 80th ed.; CRC Press: New York, 1999.

(37) Shimanouchi, T. *Tables of Molecular Vibrational Frequencies Consolidated*; National Bureau of Standards; U. S. Government Printing Office: Washinton, DC, 1972; Vol. 1.

(38) Kraka, E.; Dunning, T. H., Jr. In *Advances in Molecular Electronic Structure Theory*; Dunning, T. H., Jr., Ed.; JAI Press: Greenwich, 1990; Vol. 1.